Materials Today Physics 8 (2019) 10–17

Contents lists available at ScienceDirect

Materials Today Physics

journal homepage: https://www.journals.elsevier.com/materials-today-physics

Puzzling robust 2D metallic conductivity in undoped β-Ga_2O_3 thin films

E. Chikoidze [a,*], D.J. Rogers [b], F.H. Teherani [b], C. Rubio [c], G. Sauthier [c], H.J. Von Bardeleben [d], T. Tchelidze [e], C. Ton-That [f], A. Fellous [a], P. Bove [b], E.V. Sandana [b], Y. Dumont [a], A. Perez-Tomas [c]

[a] Groupe D'Etude de La Matière Condensée (GEMaC), Université de Versailles Saint Quentin en Yvelines – CNRS, Université Paris-Saclay, 45 Av. des Etats-Unis, 78035 Versailles Cedex, France
[b] Nanovation, 8 Route de Chevreuse, 78117 Châteaufort, France
[c] Catalan Institute of Nanoscience and Nanotechnology (ICN2), CSIC and the Barcelona Institute of Science and Technology, Barcelona, Spain
[d] Sorbonne Universités, UPMC Université Paris 6, Institut des Nanosciences de Paris, CNRS, 4, Place Jussieu, 75005 Paris, France
[e] Faculty of Exact and Natural Science, Department of Physics, Ivane Javakhishvili Tbilisi State University, 3 Av. I. Tchavtchavadze, 0179 Tbilisi, Georgia
[f] School of Mathematical and Physical Science, University of Technology Sydney, Broadway, PO Box 123, NSW 2007, Australia

ARTICLE INFO

Article history:
Received 25 October 2018
Received in revised form
16 November 2018
Accepted 16 November 2018
Available online 4 January 2019

Keywords:
Electron accumulation
Ga_2O_3
Transport properties
Wide bandgap insulator

ABSTRACT

Here, we report the analogy of an extremely stable topological-like ultra-wide bandgap insulator, a solid that is a pure insulator in its bulk but has a metallic conductive surface, presenting a two-dimensional conductive channel at its surface that challenges our current thinking about semiconductor conductivity engineering. Nominally undoped epitaxial β-Ga_2O_3 thin films without any detectable defect (after a range of state-of-the-art techniques) showed the unexpectedly low resistivity of 3×10^{-2} Ωcm which was found to be also resistant to high dose proton irradiation (2 MeV, 5×10^{15}cm^{-2} dose) and was largely invariant (metallic) over the phenomenal temperature range of 2 K up to 850 K. The unique resilience and stability of the electrical properties under thermal and highly ionizing radiation stressing, combined with the extended transparency range (thanks to the ultra-wide bandgap) and the already known toughness under high electrical field could open up new perspectives for use as expanded spectral range transparent electrodes (e.g., for UV harvesting solar cells or UV LEDs/lasers) and robust Ohmic contacts for use in extreme environments/applications and for novel optoelectronic and power device concepts.

1. Introduction

Intriguing metallic surfaces onto otherwise insulating bulk crystals have recently attracted a lot of attention [1,2]. These conductive surfaces also exhibit a number of additional unique properties such as insulator–superconductor–metal transition [3], large magnetoresistance (MR) [4], coexisting ferromagnetism and superconductivity [5], and a spin splitting of a few meV [6]. In practice, as the oxide semiconductor bandgap becomes wider, an intrinsic metallic surface is more challenging; it requires more energy to shift the Fermi level from the mid-gap to above the conduction band as the forbidden gap increases.

Beta-gallium oxide (Ga_2O_3) is an ultra-wide bandgap (UWBG) semiconductor with a highly distinctive property set compared with other classical correlated oxides such as SrTiO3 [7,8], In2O3 [9,10], CdO [11], or ZnO [12]. The uniqueness of UWBG Ga_2O_3 lies in the combination of an intrinsically wide large electrical breakdown field [13,14], ability to be efficiently donor doped [15,16], possibility to obtain low resistivity regions (even in amorphous and/or nanocrystalline states [17–20]), a high temperature *p*-type conductivity without doping [21], and 6-inch crystal low cost fabrication possibility [22]. These features have been key in promoting Ga_2O_3 to the forefront in the quest for the next generation of ultra violet C (UVC) photodetectors, solar transparent conducting electrodes, and high power/speed energy converters/switches.

Recently, the authors reported unprecedentedly high conductivity, mobility, and carrier concentration in nominally undoped thin films grown on r-sapphire substrates by pulsed laser deposition (PLD) [23].

* Corresponding author.
E-mail address: ekaterine.chikoidze@uvsq.fr (E. Chikoidze).

https://doi.org/10.1016/j.mtphys.2018.11.006
2542-5293/

This work presents evidence that the degenerate electrical conduction, in what was expected to be an insulating layer, may be due to two-dimensional–like metallic conduction in β-Ga_2O_3. Moreover, the electrical conduction has now proven stable for over two years and shows a remarkable resistance to both thermal and radiation stressing. The possibility to obtain solar blind ultra-wide bandgap undoped gallium oxide and, at the same time, highly conducting, makes this material a very fascinating transparent conducting oxide, a key-enabling material in increasingly high demand in a variety of new technologies, ranging from thin film coatings, sensors, solar cells, transparent electronics, and opto-electronics in telecommunications [24]. In addition, this analogy of an extremely stable topological-like ultra-wide bandgap insulator challenges our current thinking about semiconductor conductivity engineering.

2. Intrinsic Ga_2O_3

Nominally undoped β-Ga_2O_3 layers were grown on a 2-inch *r*-plane sapphire substrates by PLD as described in the Experimental section. The layers (~300 nm thick) were found to be epitaxial with a (201) preferential orientation. The wafers were found to be solar transparent; in that, they exhibited a large transmittance (>85%) in the UVA, UVB, and visible parts of the optical spectrum. The optical absorption edge gave an estimation of bandgap at about 240 nm (~5.2 eV). The surface and bulk chemical composition of the layers was systematically investigated by several high-resolution techniques including the following: X-ray photoemission spectroscopy (XPS), energy dispersive X-ray fluorescence spectroscopy, secondary ion mass spectroscopy (SIMS), and Rutherford backscattering spectrometry. The depth-resolved cathodoluminescence (CL) spectra of the Ga_2O_3 film with identical excitation power, shown in Fig. 5(Experimental Section), reveal a symmetrical peak at 3.3 eV. The UV emission band of the film is similar to those observed for excitons immobilized by a local lattice deformation in a single Ga_2O_3 single crystal [25]. The peak shape and energy position remain unchanged with increasing sampling depth by consequently accelerating voltage, indicating on homogeneity in sample volume. In all cases, no significant density of impurities was detected. Room temperature electron paramagnetic resonance (EPR) [26] was also performed and did not detect any shallow donor-related signal. Fig. 1 summarizes the main findings.

3. Transport properties—low temperature

The electrical transport properties of the films were studied in a van der Pauw and '4 aligned point contacts' method configurations. The room temperature resistivity (ρ (300 K)) was found to be exceptionally low for an intrinsic UWBG material (ρ (300 K) $= 3 \times 10^{-2}$ Ω cm) which is, to the best of our knowledge, the lowest reported value for undoped Ga_2O_3 thin films and about equivalent to that for heavily *n*-type–doped Ga_2O_3 (Si or Sn doping in the range of 10^{19}–10^{20} cm^{-3}) [23,25–31]. Fig. 2(a). Hall effect measurements at room temperature under 1 T revealed an electron carrier concentration as high as $n = 8.0 \times 10^{18}$ cm^{-3} for a film thickness of 200 nm and a mobility of $\mu = 19$ cm^2/V. This value of 8×10^{18} cm^{-3} corresponds to the hypothesis of thickness homogeneity of the electron carrier concentration. Such a relatively large free charge carrier concentration indicates that the Ga_2O_3 undergoes a Mott metal-insulating (M − I) transition. In Ga_2O_3, a Mott M − I transition would occur at a dopant critical concentration of $N_{Mot}t = 4 \times 10^{18}$ cm^{-3}, where $N_{Mott}^{1/3} \times a_B \approx 0.27$ and a_B is the impurity Bohr radius (a_B (Ga_2O_3) = 1.8 nm) [32]. We integrate over the film thickness; this corresponds to a surface carrier concentration of 1.6×10^{14} cm^{-2}.

Fig. 2(b) shows a representative resistance versus temperature curve measured with a colinear four-point probe configuration. The resistance was found to be relatively temperature independent (over the full range from 2 K to 400 K), and there was no evidence of carrier freeze-out at lower *T*. Both characteristics are typical signatures of metallic conduction. The slight increase of resistivity observed above 200 K is most probably attributable to a decrease in the drift mobility of free carriers. The 'hockey stick' shape with a minimum at around T_{min} ~190 K is then formed by a slight increase in resistivity at low temperatures, which is most probably due to a weak localization (WL) phenomenon which is related to low dimensional effects [33]. Owing to the quantum interference, the electron wave functions diffuse and the backscattering is enhanced which, in turn, increases the resistivity as a function of ln(*T*). As shown in Fig. 2(c), the conductivity at low temperatures increases precisely as ln(*T*) [34]. At higher temperatures, the wave coherence is progressively lost, and the WL effect gives place to metallic behavior. Similar resistivity vs *T* dependence has been already reported for confined conductive channels in two-dimensional carbides and oxides such as TiC [35], ZnO [36], $LaNiO_3$ [37], and $SrVO_3$ [38].

The WL effect is sensitive to an applied perpendicular magnetic field (*B*), which shifts T_{min} toward lower temperatures [39], as shown in Fig. 2(b). The presence of a strong magnetic field perpendicular to the plane of the conduction channel also leads to a quenching of charge localization contribution and thus produces a negative MR [40]. The MR is defined as MR = [*R*(*B*)-*R*(*B* = 0)]/*R*(*B* = 0), where *R*(*B*) is the resistance measured for *B* perpendicular to the applied current. The MR was found to be always negative at temperatures <150 K, and the maximum MR value was found to be 2.5% at *B* = 9 T (Fig. 2(d)). The field dependence up to a saturation of the negative MR at 2 K is comparable with that observed for a 2D-like conduction in highly doped semiconductors layers [40,41]. Because of the relatively small value of mobility at low temperature, quantum oscillations would not be observable even at our highest available magnetic field (9 T).

4. High temperature electrical transport properties

The metallic Ga_2O_3 conduction has been found to be stable and resistant to different stress conditions. Stored on the shelf during two years, it showed no degradation (or drift) after 10 subsequent *R*(*T*) characterization cycles. The conductive channel reversibly survived temperatures up to as high as 850 K (limit of the experimental setup), showing only a small deviation of the resistivity at elevated temperature (ρ (850 K) $= 1.7 \times 10^{-2}$ Ωcm). Analogously, the sample was proton irradiated (2 MeV, $5 \times 10^{15}$$cm^{-2}$ dose) (see experimental section) Proton irradiation at these doses and energies would be expected to create oxygen (deep donor) and gallium (deep acceptor) bulk vacancies, thus changing overall conductivity by orders of magnitude [42]. However, as shown in Fig. 2(e), the conductivity after irradiation only slightly decreases at high temperatures. As the free carrier concentration is most probably confined in a narrow region close to the surface of the layer, a metallic surface would be more resistant to radiation than bulk conductive samples where random electron-hole pairs would be formed. This high temperature stability is notable when compared with other correlated oxide systems such as confined 2D electrons metallic system $LaAlO_3$ and $SrTiO_3$ [43,44]. Single-crystal In_2O_3, ZnO, and TiO_2 have been also reported to host a surface two dimentional electron gas (2DEG) presenting however air instabilities and practical electrical conduction only at low temperature (i.e., <100 K) [45].

The resistivity versus temperature quasi-invariance stability also ruled out other known non-surface origins of intrinsic Ga_2O_3

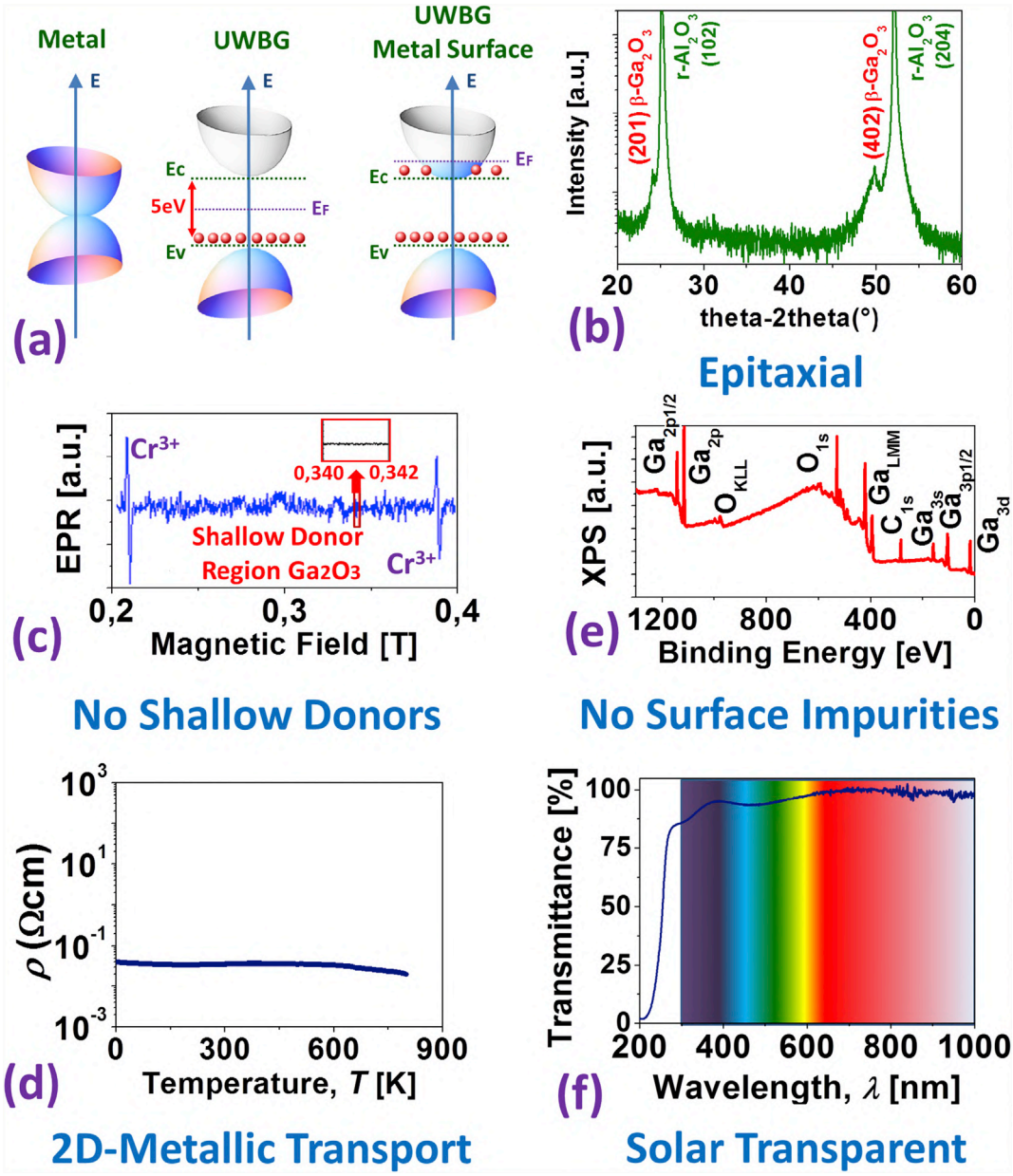

Fig. 1. (a) Sketch showing the band structure of the Ga_2O_3 conductive surface. (b) The Ga_2O_3 layers are epitaxial with (201) preferential orientation (X-ray diffraction [XRD]). There are no detectable (c) shallow donors (EPR) or (d) surface impurities (XPS). (e) The Ga_2O_3 temperature invariant metallic conductivity. (f) The Ga_2O_3 layers are solar transparent (80% transmittance in whole UVB, UVA, and visible ranges).

conductivity, i.e. the presence of (1) amorphous phases or (2) gallium clusters. Regarding (1), a chemically driven M – I Ga_2O_3 transition (of seven orders of magnitude) has been previously reported in highly non-stoichiometric, amorphous gallium oxide [46]. As we see from Fig. 2(b), *R(T)* curves showed no significant differences for subsequent heating and cooling cycles. This result excludes the possibility of solid state recrystallization reaction because of amorphous phases being present in the material. Regarding (2), gallium clusters (embedded into the Ga_2O_3 matrix) would also result in resistivity temperature hysteresis because of melting and recrystallization of Ga clusters and a sharp drop of the resistivity at low T (<10 K) (attributed to superconducting state of gallium) [47]. Furthermore, Ga clusters would render the layers non-transparent in the visible (coloration due to defects) [48]. Those features were not observed (Fig. 1d and f).

5. Electron accumulation in Ga_2O_3

The origin of the *n*-type intrinsic bulk conductivity for binary metal oxides (i.e., ZnO, In_2O_3, SnO_2, etc) is usually explained with a stoichiometric deviation: an anion (i.e., oxygen) deficiency or metallic cation interstitials. Therefore, intrinsic donors for intrinsic *n*-type conductivity in Ga_2O_3 are the oxygen vacancy, V_O and gallium interstitial, Ga_i. Hybrid functional calculations predict the V_O to be a deep donor with ionization energy higher than 1eV in Ga_2O_3. [49] Hence, it is unlikely that bulk oxygen vacancies could be the source of the metallic conductivity observed in our experiment. Interstitial Ga atom, Ga_i, are relatively shallow donors with an ionization energy of 0.1–0.2 eV. However, Ga_i has very high formation energy [50] which also makes it an unlikely candidate. Because of the breaking of translational symmetry at the surface, an

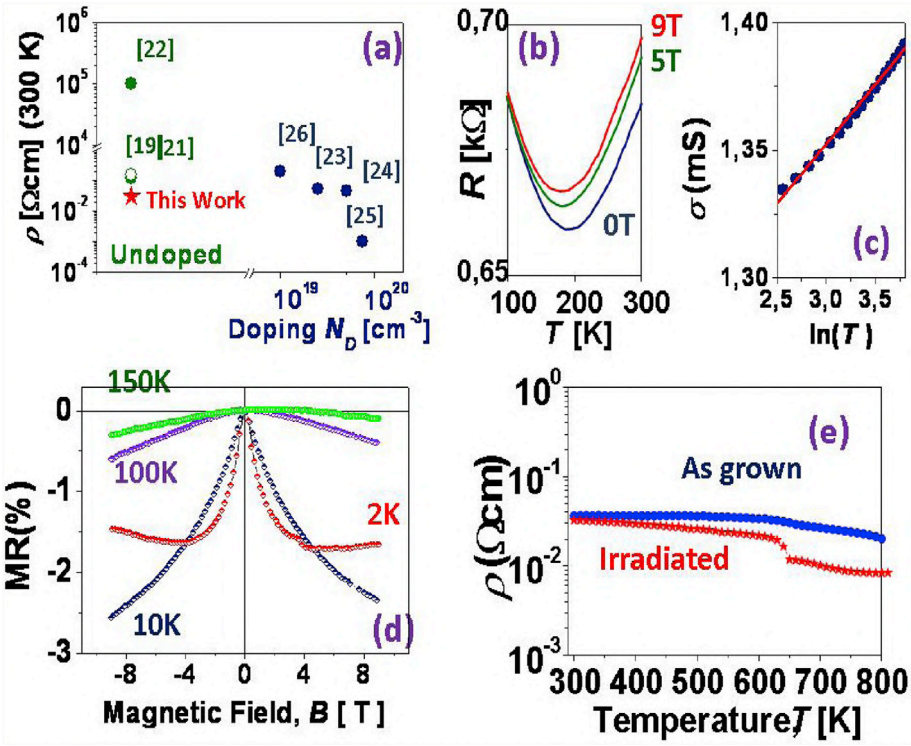

Fig. 2. (a) Room temperature resistivity for our undoped Ga_2O_3/r-sapphire sample compared with other undoped and heavily Sn- or Si-doped Ga_2O_3 results from literature [19,22–26]. (b) Zoom electrical resistance versus temperature at 0 T, 5 T, and 9 T applied magnetic fields (c) Sheet conductance σ versus ln(*T*) for uprise part below the M – I transition temperature (T_{min}) range. The solid line is the linear fit at zero magnetic field. (d) Magnetoresistance in perpendicular magnetic field at 2 K, 10 K, 100 K, and 150 K. Measurement geometry: collinear 4-point probes. (e) Electrical resistivity versus temperature (300 K–800 K) for as grown and proton irradiated (2 MeV, 5×10^{15}cm^{-2} dose) sample. Measurement configuration was carried out using the van der Pauw method.

electronic state may exist with significantly different properties and characteristic energies than those in the bulk [51]. A particularly investigated case is In_2O_3 surfaces (indirect bandgap of 2.5 eV and a direct bandgap of 3.6 eV). In_2O_3 surface donors, rather than bulk defects, are reported to be the source of its downward band-bending and surface 2DEG [52]. In a similar fashion, surface electron accumulation was also observed on the surfaces of other binary wide bandgap oxides such as CdO (E_g~2.18 eV) and ZnO (E_g~3.37 eV) [53]. In the case of Ga_2O_3, a surface band bending phenomenon due to surface defects was already pointed out by Lovejoy et al. [54]. Well-known quantum Hall Effect in 2D semiconductors and oxides usually can be observed only in high-purity Si or GaAs at very low temperatures and strong magnetic fields and at room temperature only in graphene [55].

When oxygen vacancies (or other surface donors) are present, surface positive charge causes a downward band bending; the extra electrons accumulate close to positive charges and create an accumulation layer in the near-surface region; the downward band bending causes a rigid shift of all peaks in the photoemission spectrum downward. This shift has been reported to be of 0.2–0.3 eV in the case of reduced titania which is formally associated to the transformation of Ti^{4+} to Ti^{3+} [56]. On the contrary, surface acceptors cause upward band bending, accumulation of holes close to the surface, and shift of the core levels toward lower binding energies (BE). XPS allowed the study of such core levels. The BE shifts in the O1*s* XPS spectra result from the difference in the valences of the O_2^- ions. Lower BE indicates higher electron number at O-ions. The room temperature photoemission spectrum for the Ga2*p*, Ga3*p*, O1*s*, and C1*s* core levels is shown in Fig. 3 (a). In this analysis, XPS spectra for our Ga_2O_3 layer surface (labeled *n*-type) are compared with (1) a control sample of commercial (Novel Crystal Technology, Inc.) nominally *n*-type Si-doped β-Ga_2O_3 (N_D-$N_A = 1.3 \times 10^{18}$ cm^{-3}) epitaxy (500 nm) grown on a single crystal β-Ga_2O_3 (labeled Ref) and (2) a *p*-type Ga_2O_3 surface (containing gallium vacancies) from Nanovation [21]. The BE value of the core level for the Ga2*p* states at 1119.3 eV (as determined by Michling et al. [57] for cleaved β-Ga_2O_3 single crystals) were used to calibrate the BE positions of the XPS spectra. As shown in Fig. 3(b), the Ga_2O_3 BE shift ($\Delta BE = BE\text{-}BE_{ref}$) with respect to the Si-doped Ga_2O_3 Ref correlates well with an *n*-type electron surface accumulation and a *p*-type electron depletion. The *n*-type Ga_2O_3 sample exhibits a shift toward higher BE energy values, whereas the *p*-type sample exhibits a shift toward lower BE values for both anions and cations.

Therefore, as the peaks of all elements shift the BE in the same direction, it is deduced that the BE shift is dominated by raising/lowering of the chemical potential (i.e., the potential shift due to surface oxygen vacancies or metal interstitials). It is worth mentioning that the XPS for the Ga2*p* core level spectrum show no appreciable shoulder-like feature for either Ga2$p_{1/2}$ or Ga2*p*. When the Ga_i atom occupies an interstitial site, it is surrounded by more oxygen atoms. Therefore, cationic shoulder-like features could be treated as direct evidence for the presence of interstitials. The evidence of the BE shift coupled with the absence of shoulder-like features for Ga peaks would suggest that the origin of the donors in the *n*-type layers are rather due to (surface) oxygen vacancies but which are not present on the bulk.

From valence band photoemission spectra, it is possible to determine the electronic surface properties of the thin-films. The three maxima of the O2*p* valence band correspond to the three different oxygen sites in β-Ga_2O_3 (O(1), O(2), and O(3)). The valence band width for the reference sample is ~8 eV, which is in agreement with previous reports [58]. The extrapolation of the first slope (at

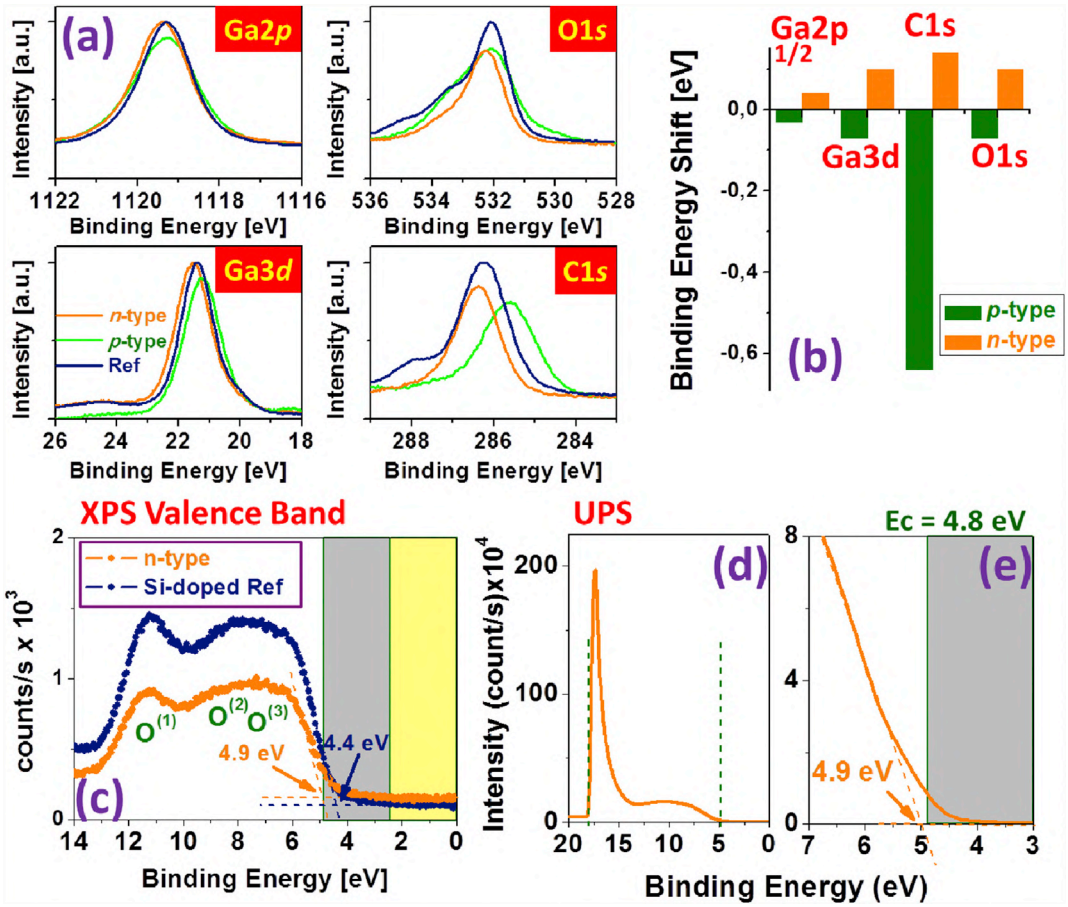

Fig. 3. (a) XPS photoemission spectra for the Ga2p, Ga3p, O1s, and C1s core levels for n-type studied sample, *p*-type [21], and Si-doped reference. (b) *n*-type and *p*-type binding energy shift ($\Delta BE = BE\text{-}BE_{ref}$) with respect to the control Si-doped Ga_2O_3. (c) Valence band photoemission spectra for *n*-type and Ref showing that our sample surface is degenerately conductive. (d) UPS spectra of the surface of the undoped conductive surface. (e) Zoom at conduction band edge. UPS, ultraviolet photoelectron spectroscopy.

~5 × 10^2 counts/s) gives Fermi levels of 4.9 eV and 4.4 eV for the Ga_2O_3 metallic surface (*n*-type) and the Si-doped control (Ref) samples, respectively. Therefore, the Fermi level for the metallic surface was experimentally confirmed to be above the conduction band edge (i.e., degenerately doped electron accumulation) if one assumes the usual bandgap value of 4.8 eV given in the literature [59]. Ultraviolet photoelectron spectroscopy (UPS) also corroborates the degenerately doped Fermi level position at ~4.9 eV as shown in Fig. 3(e).

6. Theoretical estimation of carrier accumulation

The 2DEG free electron concentration density profile can be estimated by the Thomas–Fermi approximation for a 2D system (see supplementary information) [60]. It is possible to find a relationship between the surface Fermi level (measured from the band edge) and the bulk three-dimensional electron density using:

$$E_F = \left(3\pi^2\right)^{2/3} \frac{\hbar^2}{2m_e{}^*} n^{2/3} \tag{1}$$

where E_F is the average difference between the Fermi energy and the band gap potential $V(z)$, which changes along the z-axis (the z-axis being perpendicular to the sample surface). Therefore,

$$E_F - V(z) = \left(3\pi^2\right)^{2/3} \frac{\hbar^2}{2m_e{}^*} n(z)^{2/3} \tag{2}$$

Setting the energy to zero at E_F Poisson's equation for near surface potential energy is (neglecting fixed charges):

$$\frac{d^2V}{dz^2} = \frac{1}{3\pi^2}\left(\frac{e^2}{\varepsilon_r\varepsilon_0}\right)\left(\frac{2m_e{}^*}{\hbar^2}\right)^{3/2}(-V)^{3/2} \tag{3}$$

for which solutions are,

$$V(z) = -\frac{b}{(z+z_0)^4},\ b = \left(\frac{60\pi^2\varepsilon_r\varepsilon_0}{e^2}\right)^2\left(\frac{\hbar^2}{2m_e{}^*}\right)^3 \tag{4}$$

$$n(z) = \frac{a}{(z+z_0)^6},\ a = \left(\frac{2m_e{}^*b}{\hbar^2}\right)^{3/2} \tag{5}$$

$$n(z) = \frac{a}{(z+z_0)^6},\ a = \left(\frac{2m_e{}^*b}{\hbar^2}\right)^{3/2} \tag{6}$$

In Eqs. (5) and (6), z_0 is defined by the boundary condition value of $V(0)$. Band bending at the surface *BB* was used for determining it. For *BB*:

$$BB = E^S_{v-F} - E^B_{v-f} = E^S_{v-F} - \left(E_g - E^B_{c-F}\right) \tag{7}$$

where E^S_{v-F} and E^B_{v-F} are the top of valence band to Fermi energy distance at the surface and in the bulk, respectively. The latter can be

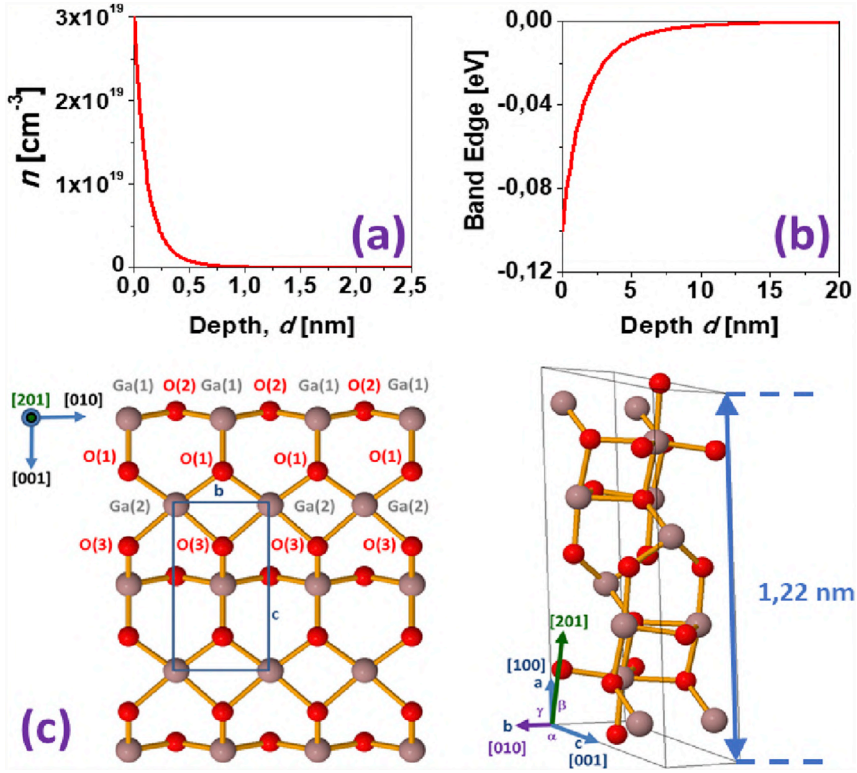

Fig. 4. (a) and (b) Simulated two-dimensional channel profile using the Thomas–Fermi approximation. (c) Sketch of the (201) plane and the Ga_2O_3 unit cell.

expressed as the sum of bulk band gap, E_g, and the distance between the Fermi energy and the bottom of conduction band in the bulk material. In Ref. [55], temperature narrowing of the bandgap in Ga_2O_3 is studied and a 4.65 eV room temperature bandgap is reported; our electron concentration corresponds to $E^B_{v-F} = 0.05\ eV$.

As the zero of energy is at E^B_{v-F}

$$V(0) = -\left(BB + E^B_{c-F}\right) = -\left(E^S_{v-F} - E_g\right) \tag{8}$$

In our case, $V(0) = -0.25eV, BB = 0.2eV$

Taking into account the experimental XPS and UPS Fermi level of 4.9 eV, an estimation of the characteristic depth profile for the bandgap potential ($V(z)$) and 2DEG density ($n(z)$) may be determined as shown in Fig. 4(a and b). The calculated concentration of surface electrons $n(0) = 10^{21}$ cm^{-3}, with an average concentration n_{av} ~ 10^{19} cm^{-3} matches well with the free electron concentration estimated in the Hall effect. The calculated electron concentration drops to ~10^{19} cm^{-3} at a depth of $z = 5$ nm, which represents roughly two Ga_2O_3 unit cells (Fig. 4(c)). Under this approximation, the sheet charge concentration of the 2DEG is n_s ~2×10^{14} cm^{-2}. Such a high value of sheet charge density induces a large diffusion of carriers and, consequently, a low value of mobility. This is the reason why no quantum oscillations are seen as a function of temperature and magnetic field in the available ranges. This may be further investigated. Nevertheless, the robust metallic conduction appears to be connected with surface band bending, as already observed in other oxide semiconductor surfaces.

7. Conclusions

In this work, temperature-dependent electrical transport measurements revealed that than nominally undoped β-Ga_2O_3, thin films exhibited degenerate metallic conduction with a room temperature Hall n of 8 × 10^{18} cm^{-3} and Hall μ of 19 cm^2/V. A number of high resolution techniques did not reveal any bulk or shallow donor signatures that could explain the conductivity in terms of conventional impurity or defect doping. The conductivity *vs* temperature was found to be unprecedentedly stable over the range from a few K to 850 K (limit of the measurement setup), both in air and nitrogen ambient and was found to be insensitive to high dose of proton irradiation (2 MeV, 5 × 10^{15}cm^{-2} dose). These suggested that the electrical conduction was mainly confined to the layer close to the surface. Photoelectron spectroscopy and hockey stick–like behavior in low temperature MR studies were also coherent with 2D conduction. The origin of a such exceptionally robust conduction merits to be investigated more deeply, because this exceptional result challenges our current understanding and methods to achieve, solar transparent conducting electrodes, Ohmic contacts, and potential transistor conductive channels in a wide bandgap insulator which is now considered to be a key enabler of a sustainable and greener future.

8. Experimental section

8.1. Fabrication details

Nominally undoped β-Ga_2O_3 layers were grown on 2-inch diameter *r*-plane sapphire substrates from a commercial sintered 4 N Ga_2O_3 target using a Coherent LPX KrF (λ = 248 nm) laser by pulsed laser deposition (PLD). Uniform 2-inch diameter wafer coverage was obtained using optical rastering of the incident laser beam. Substrate temperature during growth was measured with a thermocouple to be ~550 °C and the ambient during growth was 10^{-4} torr of molecular oxygen. Ga_2O_3 layers were epitaxial, showing (201) preferential orientation [23]. The relative low temperature (i.e. T = 500–550 °C) is enough for

Ga_2O_3 complete crystallization as reported previously by several groups [61–64]. However the crystallization temperature may vary from one set-up to another as other authors have reported that larger temperatures are required to avoid amorphous phase [65,66].

8.2. Characterization methods

8.2.1. X-ray diffraction

The crystallographic structure of the films was analyzed with a Siemens D-5000 diffractometer using Cu-K_α radiation ($\lambda = 1.54$ Å).

8.2.2. Interferometry

The thickness of the gallium oxide layers was around 300 nm, estimated using optical reflection interferometry with an Ocean Optics Nanocalc system. The layer thickness was further corroborated with cross-sectional scanning electronic microscopy (SEM) FEI Quanta 650 F Environmental SEM equipped with energy dispersive X-ray spectroscopy for point analysis and chemical maps.

8.2.3. Electron spin resonance

Electron spin resonance measurements have been performed with a Bruker X-band spectrometer under standard conditions: 100 kHz field modulation and low (μW) microwave power to avoid nuclear polarization effects. Only two transitions corresponding to a Cr contamination of the Al_2O_3 substrate were observed.

SIMS was carried out with the aid of using a Cameca IMS 4f tool equipment.

8.2.4. Cahodoluminescence

The Ga_2O_3 film was characterised by scanning CL spectroscopy using an FEI Quanta 200 SEM equipped with a parabolic mirror collector and an Ocean Optics QE65000 CCD array spectrometer. To probe defects or impurities at different depths in the film, CL spectra were acquired with different accelerating voltages between 1 and 10 kV, corresponding to a maximum excitation depth of 20–200 nm. All luminescence spectra were corrected for the total system response.

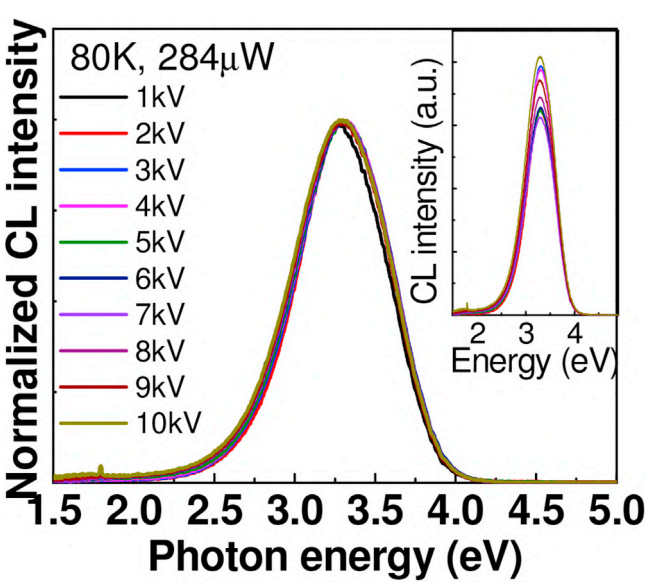

Fig. 5. Depth-resolved CL spectra showing a self-trapped exciton peak, independent of the sampling depth. CL, cathodoluminescence.

8.2.5. X-ray photoemission spectroscopy and ultraviolet photoelectron spectroscopy

X-ray photoemission spectroscopy (XPS) and UPS measurements were performed with a Phoibos 150 analyzer (SPECS GmbH, Berlin, Germany) in ultra-high vacuum conditions (base pressure 3×10^{-10} mbar). XPS measurements were performed with a monochromatic Al K_α X-ray source (1486.74 eV). UPS measurements were realized with a monochromatic HeI UV source (21.2 eV). Optical transmission spectra were measured in 200–2000 nm spectral range with a Perklin Elmer 9 spectrophotometer.

8.2.6. Transport measurements

Electrical contacts were made by soldering indium. As verified by I-V measurements, all contacts showed Ohmic I/V characteristics. Direct current (DC) resistivity and MR were studied using a commercial 'DC-resistivity' configuration in a 9 T-PPMS (Quantum Design Inc.) environment, whereas for high temperature ($T > 300$ K) measurements, a home-designed high impedance measurement setup was used. MR measurements were made with a magnetic field, $B = \mu_0 H$, applied perpendicular to the film plane. Hall effect measurements were performed in the Van der Pauw configuration for perpendicular magnetic fields of up to 1.6 T.

8.2.7. Proton irradiation

Proton irradiation was performed with a Van de Graaff 2.5 MV accelerator. A proton energy of 2 MV was chosen to generate a homogeneous defect profile over the entire film and put the end of range in the sapphire substrate. The total fluence was 1×10^{16} cm^{-2}. The current was 1 μA/cm^2, a value for which the film is expected to stay close to room temperature.

Acknowledgments

The authors acknowledge financial support from the Ile de France region ('NOVATECS' C'Nano IdF Project No? IF-08-1453. R) and from the French National Research Agency (ANR) as part of the 'Investissements d'Avenir' program (Labex charmmmat, ANR-11-LABX-0039-grant). APT acknowledges Agencia Estatal de Investigación (AEI) and Fondo Europeo de Desarrollo Regional under contract ENE2015-74275-JIN. The ICN2 is funded by the Centres de Recerca de Catalunya (CERCA) programme/Generalitat de Catalunya and by the Severo Ochoa programme of the Spanish Ministry of Economy, Industry and Competitiveness (MINECO, grant no. SEV-2013-0295). TT acknowledges Shota Rustaveli National Science Foundation, grant #04/04.

The authors express their thanks to Dr. F. Jomard (GEMaC laboratory,CNRS-UVSQ) for SIMS measurements.

References

[1] E.S. Reich, Hopes surface for exotic insulator, Nature 13 (2012) 492.
[2] T.C. Rödel, F. Fortuna, S. Sengupta, Emmanouil Frantzeskakis, P. Le Fèvre, F. Bertran, B. Mercey, Sylvia Matzen, G. Agnus, T. Maroutian, P. Lecoeur, A.F. Santander-Syro, Universal fabrication of 2D electron systems in functional oxides, Adv. Mater. 28 (2016) 1976.
[3] J. He, D. Di Sante, R. Li, X.-Q. Chen, J.M. Rondinelli, C. Franchini, Tunablemetal-Insulator transition, Rashba effect and Weyl Fermions in a relativistic charge-ordered ferroelectric oxide, Nat. Commun. 9 (2018) 492.
[4] R. von Helmolt, J. Wecker, B. Holzapfel, L. Schultz, K. Samwer, Giant negative magnetoresistance in perovskitelike La2/3Ba1/3MnOx ferromagnetic films, Phys. Rev. Lett. 71 (1993) 2331.
[5] J.G. Bednorz, K.A. Muller, Perovskite-type oxides—the new approach to high-Tc superconductivity, Rev. Mod. Phys. 60 (1988) 585.
[6] A.F. Santander-Syro, F. Fortuna, C. Bareille, T.C. Rödel, G. Landolt, N.C. Plumb, J.H. Dil, M. Radović, Giant spin splitting of the two-dimensional electron gas at the surface of $SrTiO_3$, Nat. Mater. 13 (2014) 1085.
[7] Yuhang Wang, Kehan Zhao, Xiaolan Shi, Li Geng, Guanlin Xie, Xubo Lai, Jun Ni, Liuwan Zhang, Mechanical writing of n-type conductive layers on the $SrTiO_3$ surface in nanoscale, Sci. Rep. 5 (2015) 10841.

[8] D.S. Deak, Strontium titanate surfaces, Mat. Sci. Technol. 23 (2007) 127.
[9] D.R. Hagleitner, M. Menhart, P. Jacobson, S. Blomberg, K. Schulte, E. Lundgren, M. Kubicek, J. Fleig, F. Kubel, C. Puls, A. Limbeck, H. Hutter, L.A. Boatner, M. Schmid, U. Diebold, Bulk and surface characterization of In_2O_3(001) single crystals, Phys. Rev. B 85 (2012) 115441.
[10] P. Agoston, P. Erhart, A. Klein, K. Albe, Geometry, electronic structure and thermodynamic stability of intrinsic point defects in indium oxide, J. Phys. Condens.Matt. 21 (2009) 455801.
[11] J. Santos-Cruz, G. Torres-Delgado, R. Castanedo-Perez, S. Jiménez-Sandoval, O. Jiménez-Sandoval, C.I. Zúñiga-Romero, J. Márquez Marín, O. Zelaya-Angel, Optical and electrical characterization of fluorine doped cadmium oxide thin films prepared by the sol–gel method, Thin Solid Films 515 (2007) 5381.
[12] G. Luka, T. Krajewski, L. Wachnicki, B. Witkowski, E. Lusakowska, W. Paszkowicz, E. Guziewicz, M. Godlewski, Transparent and conductive undoped zinc oxide thin films grown by atomic layer deposition, Phys.Stat.sol. 207 (2010) 1568 (a).
[13] M. Higashiwaki, K. Sasaki, A. Kuramata, T. Masui, S. Yamakoshi, Gallium oxide (Ga_2O_3) metal-semiconductor field-effect transistors on single-crystal β-Ga_2O_3 (010) substrates Appl, Phys. Lett. 100 (2012), 013504.
[14] A.J. Green, K.D. Chabak, M. Baldini, N. Moser, R. Gilbert, R.C. Fitch, G. Wagner, Z. Galazka, J. McCandless, A. Crespo, K. Leedy, G.H. Jessen, β-Ga_2O_3MOSFETs for radio frequency operation, IEEE Electron. Device Lett. 38 (2017) 790.
[15] S.I. Stepanov, V.I. Nikolaev, V.E. Bourgov, A.E. Romanov, Gallium oxide: properties and application, Rev. Adv. Mater. Sci. 44 (2016) 63.
[16] S.J. Pearton, J. Yang, P.H. Cary, F. Ren, J. Kim, M.J. Tadjer, M.A. Mastro, A review of Ga_2O_3 materials, processing, and devices, Appl. Phys. Rev. 5 (2018), 011301.
[17] L.I. Juarez-Amador, M. Galvan-Arellano, J.a. Andraca-Adame, G. Romero-paredas, A. kennedy-Magos, R. Pena-sierra, J.Mater. Sci.:Mater.in Electron. 18 (2018) 1.
[18] C.V. ramana, E.J. Rubio, C.D. Barraza, a. Miranda Gallardo, S. McPeack, S. Kortu, J.T. Grant, J. Appl. Phys. 115 (2014), 043508.
[19] M.D. Heinemann, J. Berry, G. Teeter, T. Unold, D. Ginley, Oxygen deficiency and Sn doping of amorphous Ga_2O_3, Appl. Phys. Lett. 108 (2016), 022107.
[20] J. Kim, T. Sekiya, N. Miyokawa, N. Watanabe, K. Kimoto, K. Ide, Y. Toda, Sh Ueda, N. Ohashi, H. Hiramatsu, H. Hosono, Conversion of an ultra-wide bandgap amorphous oxide insulator to a semiconductor, NPG Asia Mater. 9 (2017) e359.
[21] E. Chikoidze, A. Fellous, A. Perez-Tomas, G. Sauthier, T. Tchelidze, C. Ton-That, T. Thanh Huynh, M. Phillips, S. Russell, M. Jennings, B. Berini, F. Jomard, Y. Dumont, P-type β-gallium oxide: a new perspective for power and opto-electronic devices, Mater. Today Phy. 3 (2017) 118.
[22] M. Orita, H. Hiramatsu, H. Hosono, Preparation of highly conductive, deep ultraviolet transparent β-Ga_2O_3 thin film at low deposition temperatures, Thin Sol.Films 411 (2002) 134.
[23] F.H. Teherani, D.J. Rogers, V.E. Sandana, P. Bove, C. Ton-That, L.L.C. Lem, E. Chikoidze, M. Neumann-Spallart, Y. Dumont, T. Huynh, M.R. Phillips, P. Chapon, R. McClintock, M. Razeghi, Investigations on the substrate dependence of the properties in nominally-undoped β-Ga_2O_3 thin films grown by PLD, Proc. SPIE 10105 (2017) 10105R.
[24] R.M. Pasquarelli, David S. Ginley, O'Hayre Ryan, Solution processing of transparent conductors: from flask to film, Chem. Soc. Rev. 40 (2011) 5406.
[25] K. Shimamura, E.G. Villora, T. Ujiie, K. Aoki, Excitation and photoluminescence of pure and Si-doped β-Ga_2O_3 single crystals, Appl. Phys. Lett. 92 (2008) 201914.
[26] M. Yamaga, E.G. Víllora, K. Shimamura, N. Ichinose, M. Honda, Donor structure and electric transport mechanism in β–Ga_2O_3, Phys. Rev. B 68 (2003) 155207.
[27] Sin-Liang Ou, Dong-Sing Wuu, Yu-Chuan Fu, Shu-Ping Liu, Feng Zhe-Chuan, Growth and etching characteristics of gallium oxide thin films by pulsed laser deposition, Mat.chem.Phys 133 (2012) 700.
[28] K. Matsuzaki, H. Hiramatsu, K. Nomura, H. Yanagi, T. Kamiya, M. Hirano, H. Hosono, Preparation of highly conductive, deep ultraviolet transparent β-Ga_2O_3 thin film at low deposition temperatures, Thin Solid Films 496 (2006) 37.
[29] Mi Wei, Du Xuejian, Luan Caina, Xiao Hongdi, Ma Jin, Electrical and optical characterizations of β-Ga_2O_3:Sn films deposited on MgO (110) substrate by MOCVD, RSC Adv. 4 (2014) 30579.
[30] N. Suzuki, S. Ohira1, M. Tanaka, T. Sugawara, K. Nakajima, T. Shishido, Fabrication and characterization of transparent conductive Sn–doped β–Ga_2O_3 single crystal phys, stat. sol.C 4 (2007) 2310.
[31] Kevin D. Leedy, Kelson D. Chabak, V. Vasilyev, D.C. Look, J.J. Boeckl, J.L. Brown, S.E. Tetlak, A.J. Green, N.A. Moser, A. Crespo, D.B. Thomson, R.C. Fitch, J.P. McCandless, G.H. Jessen, Highly conductive homoepitaxial Si-doped Ga_2O_3 films on (010) β-Ga_2O_3 by pulsed laser deposition, Appl. Phys. Lett. 111 (2017), 012103.
[32] E. Chikoidze, H.J. von Bardeleben, K. Akaiwa, E. Shigematsu, K. Kaneko, S. Fujita, Y. Dumont, Electrical, optical, and magnetic properties of Sn doped α-Ga2O3 thin films, J. Appl. Phys. 120 (2016), 025109.
[33] G. Herranz, F. Sanchez, B. Martınez, J. Fontcuberta, M.V. Garcıa-Cuenca, C. Ferrater, M. Varela, P. Levy, Eur. Phys. J. B40 (2004) 439.
[34] Z.Q. Liu, D.P. Leusink, X. Wang, W.M. Lü, K. Gopinadhan, A. Annadi, Y.L. Zhao, X.H. Huang, S.W. Zeng, Z. Huang, A. Srivastava, S. Dhar, T. Venkatesan, Ariando, Phys. Rev. Lett. 107 (2011) 146802.
[35] J. Halim, M.R. Lukatskaya, K.M. Cook, J. Lu, C.R. Smith, L.-A. Näslund, S.J. May, L. Hultman, Y. Gogotsi, P. Eklund, M.W. Barsoum, Chem. Mater. 26 (2014) 2374.
[36] M. Nistor, F. Gherendi, N.B. Mandache, C. Hebert, J. Perriere, W. Seiler, Metal-semiconductor transition in epitaxial ZnO thin films, J. Appl. Phys. 106 (2009) 103710.
[37] W. Noun, B. Berini, Y. Dumont, P.R. Dahoo, N. Keller, Correlation between electrical and ellipsometric properties on high-quality epitaxial thin films of the conductive oxide $LaNiO_3$ on STO (001), J. Appl. Phys. 102 (2007), 063709.
[38] M. Gu, S.A. Wolf, J. Lu, Two-dimensional Mott insulators in $SrVO_3$ ultrathin films, Adv. Mater. Interfaces (2014) 1300126.
[39] E. Rozenberg, M. Auslender, I. Felner, G. Gorodetsky, Low-temperature resistivity minimum in ceramic manganites, J. Appl. Phys. 88 (2000) 2578.
[40] S. Ashburn, R.A. Webb, E.E. Mendez, L.L. Chang, L. Esaki, Phys. Rev. 29 (1984) 3752.
[41] S. Kawaji, Weack localization and and negative magnetoresistance in semiconductor two-dimensional systems, Surf. Sci. 170 (1986) 682.
[42] S. Ahn, Y.-H. Lin, F. Ren, S. Oh, Y. Jung, G. Yang, J. Kim, M.A. Mastro, J.K. Hite, Ch.R. Eddy, Stephen Jr., J. Pearton, J. Vac. Sci. Technol. B 34 (2016), 041213.
[43] S.Y. Moon, Ch.W. Moon, H.J. Chang, T. Kim, Ch-Y. Kang, H.-J. Choi, J.-S. Kim, S.-Hyub Baek, H.W. Jang, Thermal stability of 2DEG at amorphous $LaAlO_3$/crystalline $SrTiO_3$ heterointerfaces, Nano Convergence 12 (2016) 243.
[44] M. Huijben, A. Brinkman, G. Koster, G. Rijnders, H. Hilgenkmp, D.H.A. Blank, Structure-Property relation of $SrTiO_3$/$LaAlO_3$ interfaces, Adv.Mater. 21 (2009) 1665.
[45] Lee Sang Yeon, J. Kim, A. Park, J. Park, H. Seo, Creation and control of two-dimensional electron gas using Al-based amorphous oxides/$SrTiO_3$ heterostructures grown by atomic layer deposition, ACS Nano 11 (2017) 6040.
[46] L. Nagarajan, R.A. De Souza, D. Samuelis, I. Valov, A. Börger, J. Janek, K. Becker, P.C. Schmidt, M. Martin, A chemically driven insulator-metal transition in non-stoichiometric and amorphous gallium oxide, Nat. Mater. 7 (2008) 391.
[47] C. Hebert, A. Petitmangin, J. Perrière, E. Millon, A. Petit, L. Binet, P. Barboux, Mater. Chem. Phys. 133 (2012) 135.
[48] A. Petitmangin, B. Gallas, C. Hebert, J. Perriere, L. Binet, P. Barboux, X. Portier, Characterization of oxygen deficient gallium oxide films grown by PLD, Appl. Surf. Sci. 278 (2013) 153.
[49] J.B. Varley, J.R. Weber, A. Janotti, C.G. Van de Walle, J. Appl. Phys. Lett. 97 (2010) 142106.
[50] V. Wang, W. Xiao, L.-J. Kang, R.-J. Liu, H. Mizuseki, Y. Kawazoe, Sources of n-type conductivity in $GaInO_3$, J. Phys. D Appl. Phys. 48 (2015), 015101.
[51] P.D.C. King, T.D. Veal, C.F. McConville, J. Zuñiga-Pérez, V. Muñoz-Sanjosé, M. Hopkinson, E.D.L. Rienks, M. Fuglsang Jensen, Ph. Hofmann, Surface band-gap narrowing in quantized electron accumulation layers, PRL 104 (2010) 256803.
[52] D. Phil, C. King, T. D Veal, Conductivity in transparent oxide semiconductors, J. Phys. Condens. Matter 23 (2011) 334214.
[53] S. Lany, A. Zakutayev, T.O. Mason, J.F. Wager, K.R. Poeppelmeier, J.D. Perkins, J.J. Berry, D.S. Ginley, A. Zunger, Surface origin of high conductivities in undoped In_2O_3 thin films, Phys.Rev.Lett. 108 (2012), 016802.
[54] T.C. Lovejoy, R. Chen, X. Zheng, E.G. Villora, K. Shimamura, H. Yoshikawa, Y. Yamashita, S. Ueda, K. Kobayashi, S.T. Dunham, F.S. Ohuchi, M.A. Olmstead, Band bending and surface defects in β-Ga_2O_3Appl, Phys. Lett. 100 (2012) 181602.
[55] J. Wang, F. Ma, W. Liang, M. Sun, Mater. Today Phy. 2 (2017) 6.
[56] J. Jupille, G. Thornton (Eds.), Defects at Oxide Surfaces, Springer, Heidelberg, 2015.
[57] M. Michling, D. Schmeißer, Resonant Photoemission at the O1s threshold to characterize β-Ga_2O_3 single crystals, IOP Conf. Ser. Mater. Sci. Eng. 34 (2012), 012002.
[58] C. Janowitz, V. Scherer, M. Mohamed, A. Krapf, H. Dwelk, R. Manzke, Z. Galazka, R. Uecker, K. Irmscher, R. Fornari, New J. Phys. 13 (2011), 085014.
[59] Low-dimensional Semiconductor Structures: Fundamentals and Device Applications, by Keith Barnham, Dimitri Vvedensky, Cambridge University Press, Cambridge; New York, 1943, p. 393.
[60] S. Rafique, L. Han, Sh. Mou, H. Zhao, Temperature and doping concentration dependence of the energy band gap in β-Ga_2O_3 thin films grown on sapphire, Opt. Mater. Express 7 (2017) 3561.
[61] F. Zhang, Li Haiou, Cui Yi-Tao, Guo-Ling Li,Qixin Guo ,evolution of optical properties and band structure from amorphous to crystalline Ga_2O_3 films, AIP Adv. 8 (2018), 045112.
[62] Ou Sin-Liang, Wuu Dong-Sing, Fu Yu-Chuan, Liu Shu-Ping, Horng Ray-Hua, Liu Lei, Feng Zhe-Chuan, Growth and etching characteristics of gallium oxide thin films by pulsed laser deposition, Mater. Chem. Phys. 133 (2012) 700.
[63] F.B. Zhang, K. Saito, T. Tanaka, M. Nishio, Q.X. Guo, Structural and optical properties of Ga_2O_3 films on sapphire substrates by pulsed laser deposition, J. Cryst. Growth 387 (2014) 96.
[64] K. Matsuzaki, H. Hiramatsu, K. Nomura, H. Yanagi, Growth, structure and Carrier transport properties of Ga_2O_3 epitaxial film examined for transparent field-effect transistor, Thin Solid Films 496 (2000) 37.
[65] D. Guo, Z. Wu, P. Li, Y. An, H. Liu, X. Guo, H. Yan, G. Wang, C. Sun, L. Li, W. Tang, Fabrication of β-Ga_2O_3 thin films and solar-blind photodetectors by laser MBE technology, Opt. Mater. Expr. 4 (2014) 106.
[66] D.Y. Guo, Y.P. Qian, Y.L. Su, H.Z. Shi, P.G. Li, J.T. Wu, S.L. Wang, C. Cui, W.H. Tang, Evidence for the bias-driven migration of oxygen vacancies in amorphous non-stoichiometric gallium oxide, AIP Adv. 7 (2017), 065312.